

# Addressing Limitations with the MM-GB/SA Scoring Procedure using the WaterMap Method and Free Energy Perturbation Calculations

Cristiano R. W. Guimarães\* and Alan M. Mathiowetz

CVMD Chemistry, PharmaTherapeutics Research and Development, Pfizer, Inc., 558 Eastern Point Road, Groton, Connecticut 06340

Received December 22, 2009

The MM-GB/SA scoring technique has become an important computational approach in drug design. We, and others, have demonstrated that for congeneric molecules the correlation with experimental data obtained with the physics-based scoring is usually superior to scoring functions from typical docking algorithms. Despite showing good accuracy when applied within a series, much work is necessary to improve the MM-GB/SA method in order to gain greater efficiency in drug design. Here, we investigate the poor estimation of protein desolvation provided by the GB/SA solvation model and the large dynamic range observed in the MM-GB/SA scoring compared to that of the experimental data. In the former, replacing the GB/SA protein desolvation in the MM-GB/SA method by the free energy associated with displacing binding site waters upon ligand binding estimated by WaterMap provides the best results when ranking congeneric series of factor Xa and cyclin-dependent kinase 2 (CDK2) inhibitors. However, the improvement is modest over results obtained with the MM-GB/SA and WaterMap methods individually, apparently due to the high correlation between the free energy liberation of the displaced solvent and the protein–ligand van der Waals interactions, which in turn may be interpretable as estimates of the hydrophobic effect and hydrophobic-like interactions, respectively. As for the large dynamic range, comparisons between MM-GB/SA and FEP calculations indicate that for the factor Xa test set this problem has its origin in the lack of shielding effects of protein–ligand electrostatic interactions; that overly favors ligands that engage in hydrogen bonds with the protein.

## INTRODUCTION

The combination of molecular mechanics and the Poisson–Boltzmann (PB) continuum solvation to compute binding free energies was pioneered by Kollman and co-workers.<sup>1a</sup> The encouraging results obtained with this methodology, despite limitations,<sup>1b</sup> inspired several authors to use molecular mechanics-based scoring functions with the generalized Born model<sup>2</sup> as the implicit solvent (MM-GB/SA) in the rescoring of docking poses.

Despite the great size and complexity of the conformational space of typical ligands, different docking methodologies, e.g., force field, empirical, and knowledge based, have all been successful in reproducing the crystallographic binding modes.<sup>3–7</sup> However, they all struggle when it comes to predicting binding affinities,<sup>8–12</sup> particularly the scoring function terms responsible for the estimation of the ligand desolvation, intramolecular strain, and conformational entropy penalties upon binding. When compared to docking scoring functions, the MM-GB/SA procedure provides improved enrichment in the virtual screening of databases and better correlation between calculated binding affinities and experimental data.<sup>13</sup> The MM-GB/SA rescoring method, however, performs poorly in some cases, suggesting that success through its application may be system dependent.<sup>13i,j</sup>

More recently, we investigated the performance of our MM-GB/SA version when rescoring docking poses of

congeneric series against their respective targets cyclin-dependent kinase 2 (CDK2), factor Xa, thrombin, and HIV-RT.<sup>13h</sup> The correlation with experiment obtained with the physics-based scoring was far superior to the one obtained with the Glide 4.0 XP scoring function.<sup>6,14</sup> The remarkable results for all systems even qualify the MM-GB/SA approach as a more attractive alternative for rank ordering than the more rigorous, but computationally intensive, FEP and TI methodologies;<sup>15–20</sup> it can achieve equivalent predictive accuracy, handle more structurally dissimilar ligands, and provide results at a fraction of the computational cost.

In our MM-GB/SA implementation, the protein desolvation term described by the GB/SA model is excluded from the scoring because it generally deteriorates the results (see Results and Discussion Section); the geometry optimization of the protein–ligand complexes, however, is performed in the presence of solvation effects. A possible explanation for this is that the continuum solvation model does not describe the underlying physics for such complex systems with sufficient accuracy to reliably estimate the different protein desolvation free energies resulting from the binding of each ligand. The explicit consideration of water molecules in protein binding sites is then an interesting alternative to improve the quality of scoring methods that are based on the implicit description of solvent effects.

The ability to predict the structural and thermodynamic properties of water molecules in protein binding sites has been investigated by numerous theoretical methods.<sup>21</sup> Early studies were mainly based on free energy simulations that

\* Corresponding author. Telephone: (860) 686-2915. E-mail: cristiano.guimaraes@pfizer.com.

compute the absolute binding free energy of a water molecule at a putative location.<sup>21a–e</sup> Their main obstacle was the number of simulations needed to compute the absolute binding free energy of many water molecules. To address this limitation, Michel and co-workers recently developed a method called JAWS that is far more efficient than conventional free energy simulations.<sup>21f</sup> Among other recent efforts is the one by Abel and co-workers who developed a method called WaterMap.<sup>21g–i</sup> In this method, the hydration site locations in the binding site cavity are obtained using a clustering technique applied to a molecular dynamics (MD) simulation of explicit water molecules solvating a rigid protein structure. The thermodynamic properties of the hydration sites, specifically enthalpy and entropy changes with respect to bulk water, are obtained from the averaging of solvent–solvent and protein–solvent interaction energies and the application of the inhomogeneous solvation theory, respectively. A displaced solvent functional was later derived to estimate the free energy liberation when a ligand that is suitably complementary to the binding site displaces the waters therein into an assumed-to-preexist cavity in bulk solution, previously occupied by the ligand. As a consequence, a cavity of identical size and shape is formed in the protein. The WaterMap method then represents an attempt to isolate the free energy associated with transferring the solvent cavity from the bulk to the binding site from all other contributions to binding and provides, in other words, an estimate for the hydrophobic effect.

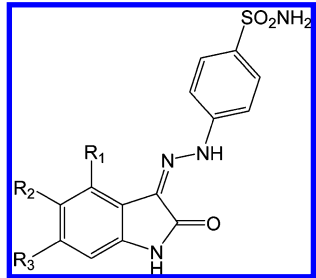
In WaterMap, protein and ligand entropic changes and intramolecular strain upon binding as well as ligand–solvent and protein–ligand interaction energies are excluded from the free energy liberation estimate; our MM-GB/SA approach includes most of them in the scoring. On the other hand, WaterMap does include the loss of protein–solvent interactions when the cavity is created in the binding site, a term that is not reliably computed by the continuum solvation model. Therefore, WaterMap and MM-GB/SA seem rather complementary methodologies. Because of that, and given the previous successes of WaterMap,<sup>21h,i</sup> we decided to investigate the benefit of combining it with our MM-GB/SA scoring equation.

Out of the four targets studied in our previous account,<sup>13h</sup> CDK2 and factor Xa with their respective congeneric series were used in this work as test cases.<sup>22,23</sup> They provide examples of pharmaceutically relevant targets and chemical matter that is typically generated during the exploration of structure–activity relationships. Their congeneric series also contain a reasonable number of compounds as well as activity data covering three orders of magnitude. MM-GB/SA calculations, using the original implementation<sup>13h</sup> and augmented by WaterMap calculations, were performed and the results compared to the experimental data. In addition, FEP calculations were run for selected pairs of factor Xa inhibitors to analyze additional limitations with the current MM-GB/SA methodology.

## METHODS

**Docking.** The crystal structures for CDK2 and factor Xa complexed with the inhibitors indirubin-5-sulfonate (PDB ID: 1E9H) and ZK-807834 (PDB ID: 1FJS), respectively, were employed in the docking calculations performed by

**Table 1.** Enzymatic Activities of Selected CDK2 Inhibitors (Core 1)



R <sub>1</sub>	R <sub>2</sub>	R <sub>3</sub>	IC <sub>50</sub> (nM) <sup>a</sup>
H	H	H	120
CH <sub>2</sub> CH <sub>3</sub>	H	H	7.9
CH(CH <sub>3</sub> ) <sub>2</sub>	H	H	2.5
CH <sub>2</sub> CH(CH <sub>3</sub> ) <sub>2</sub>	H	H	1.2
OCH(CH <sub>3</sub> ) <sub>2</sub>	H	H	3.4
OPh	H	H	13
NO <sub>2</sub>	H	H	2400
H	F	H	34
H	Cl	H	43
H	Br	H	60
H	CH <sub>3</sub>	H	46
H	OCH <sub>3</sub>	H	12
H	NH <sub>2</sub>	H	74
H	SO <sub>2</sub> CH <sub>3</sub>	H	16
H	SO <sub>2</sub> NH <sub>2</sub>	H	43
H	CONH <sub>2</sub>	H	4.5
H	CON(CH <sub>3</sub> ) <sub>2</sub>	H	17
H	H	Br	43
H	H	CH <sub>2</sub> CH <sub>3</sub>	21
H	H	CH(CH <sub>3</sub> ) <sub>2</sub>	75
Cl	CH <sub>3</sub>	H	13
Cl	OCH <sub>3</sub>	H	54
CH <sub>3</sub>	NO <sub>2</sub>	H	4.6

<sup>a</sup> Ref 22.

Glide.<sup>6,14</sup> Although there is a complex between CDK2 and an inhibitor belonging to the selected congeneric series (Table 1) available in the Protein Data Bank (PDB ID: 1FVT), this structure is not consistent with the conditions for the biological assay; it is not complexed to cyclin A nor is it phosphorylated on Thr160. Figure 1a and b illustrate the differences between the 1FVT and 1E9H CDK2 structures. The absence of cyclin A and Thr160 phosphorylation in 1FVT cause a repositioning of the C-helix and a major conformational change on the activation loop that render CDK2 inactive. The inhibitor indirubin-5-sulfonate in 1E9H, however, does not have the sulfonamide group that is sandwiched between the D86 and K89 residues, like in the 1FVT complex. The absence of this interaction causes a conformational change on Q85 and K89. Since the series of selected CDK2 inhibitors (Tables 1 and 2) display this interaction with the enzyme, the Q85 and K89 side-chain conformations in 1E9H were changed to reflect the conformation adopted in the 1FVT crystal structure. After that, the inhibitor in 1FVT was optimally overlaid in the modified 1E9H binding site, and the generated complex was used as starting point in the CDK2 docking calculations (Figure 1c). All complexes were submitted to a series of restrained, partial minimizations using the OPLS\_2005 force field.<sup>24,25</sup> Before the docking calculations, the selected congeneric series of CDK2<sup>22</sup> and factor Xa<sup>23</sup> inhibitors shown in Tables 1–3 were submitted to a pre-energy minimization using both the OPLS\_2005 force field and the GB/SA method as the

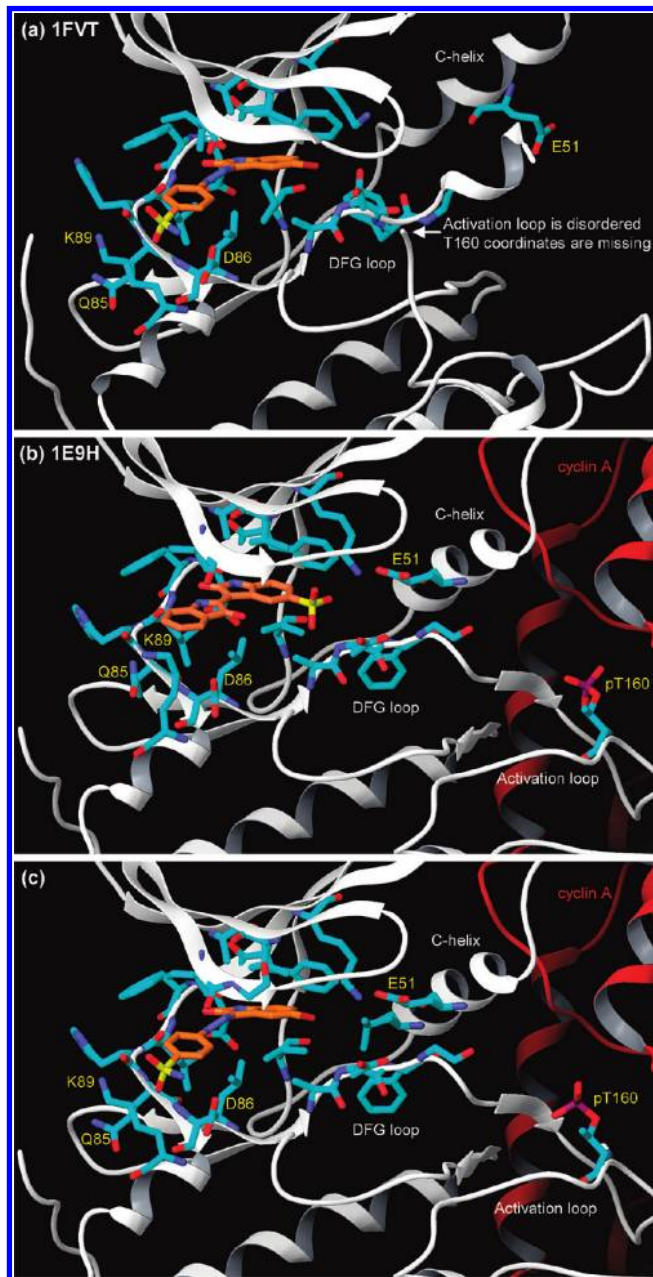
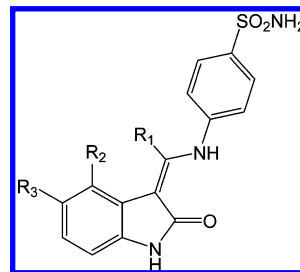


**Figure 1.** (a) 1FVT and (b) 1E9H crystal structures between CKD2 and inhibitors. (c) Modified 1E9H structure complexed to the 1FVT inhibitor used in the docking calculations.

implicit water model.<sup>2</sup> In order to accommodate the fact that the protein structure used for docking will not, in general, be optimized to fit a particular ligand, the van der Waals (vdW) radii for nonpolar protein atoms were scaled by a factor of 0.8, while those for the ligands were not scaled. The Glide 5.0 XP scoring function was used in this work.<sup>26</sup>

**MM-GB/SA Rescoring.** In our implementation of the MM-GB/SA rescoring (Figure 2), described in details in ref 13h, a conformational search for the inhibitors in the unbound state and energy minimization for the complexes using OPLS\_2005 and GB/SA within MacroModel<sup>27</sup> are performed. All conformers within 5.0 kcal/mol from the lowest-energy conformer were retained. Assuming a Boltzmann distribution, the probability for each conformer ( $P_i$ ) was calculated and used to compute the Boltzmann-averaged intramolecular energy and the solvation free energy in the

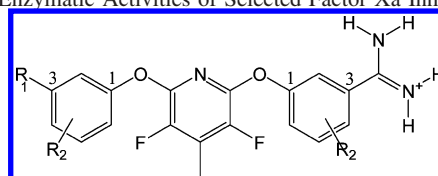
**Table 2.** Enzymatic Activities of Selected CDK2 Inhibitors (Core 2)



R <sub>1</sub>	R <sub>2</sub>	R <sub>3</sub>	IC <sub>50</sub> (nM) <sup>a</sup>
H	H	H	690
CH <sub>3</sub>	H	H	360
CH <sub>3</sub>	H	Cl	22
H	CH <sub>2</sub> OH	H	54
H	H	N(CH <sub>3</sub> ) <sub>2</sub>	310
H	H	COOCH <sub>3</sub>	2.1

<sup>a</sup> Ref 22.

**Table 3.** Enzymatic Activities of Selected Factor Xa Inhibitors



R <sub>1</sub>	R <sub>2</sub>	R <sub>3</sub>	K <sub>i</sub> (nM) <sup>a</sup>
CONH <sub>2</sub>	H	H	280
CONHMe	H	H	1200
COMe	H	H	1400
NH <sub>2</sub>	H	H	3300
NMe <sub>2</sub>	H	H	160
NHEt	H	H	530
OMe	H	H	1350
OCF <sub>3</sub>	H	H	1800
F	H	H	3200
Cl	H	H	1700
OH	H	H	5000
CF <sub>3</sub>	H	H	1600
CONMe <sub>2</sub>	5-OMe	H	140
NMe <sub>2</sub>	2-Me	H	320
CONMe <sub>2</sub>	H	6-NH <sub>2</sub>	14
CONMe <sub>2</sub>	H	6-OH	1.8
NMe <sub>2</sub>	H	6-Me	1200
NMe <sub>2</sub>	H	6-NH <sub>2</sub>	64
NMe <sub>2</sub>	H	6-OH	3

<sup>a</sup> Ref 23.

unbound state for each compound. The conformational entropies ( $S_{\text{conf}}$ ) were computed from the probabilities using eq 1, where  $k_B$  is the Boltzmann constant.

$$S_{\text{conf}} = -k_B \sum_{i=1}^n P_i \ln P_i \quad (1)$$

To better account for the protein flexibility, the best pose for each inhibitor was energy minimized in the bound state. In the energy minimization, no constraints were applied to residues within 5 Å from the center of the system. A second shell of 3 Å around the first shell was defined, and constraints of 50 kcal/mol·Å<sup>2</sup> were applied to the residues therein. The remaining residues were held fixed. After the energy minimization step, the protein energy ( $E_{\text{ptm}}$ ) values for all



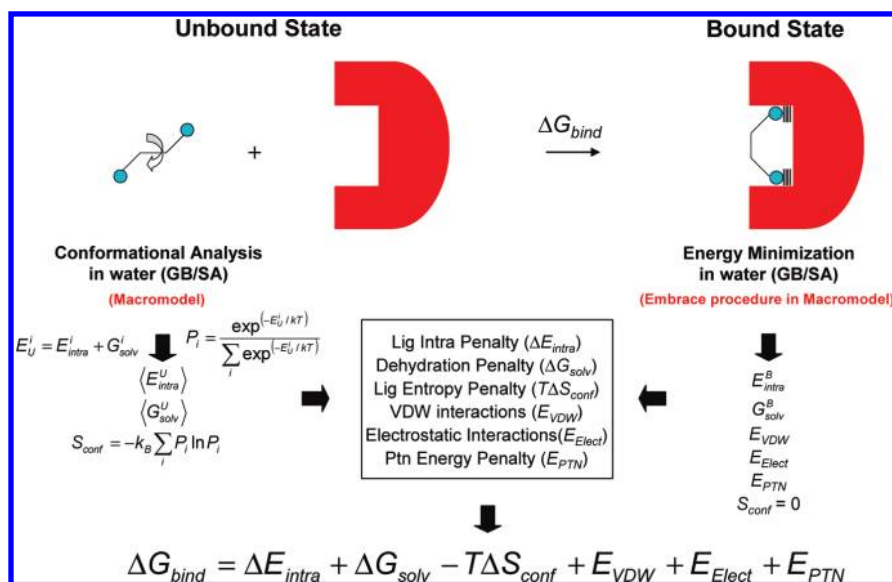


Figure 2. Schematic representation of the MM-GB/SA rescoring procedure with no protein desolvation term.

complexes were extracted. This term describes the protein deformation or the strain imposed by each ligand. Besides  $E_{\text{ptn}}$ , the energy-minimized structures for the complexes provided the intramolecular and the solvation free energies for the ligands in the protein environment, the protein–ligand intermolecular van der Waals ( $E_{\text{vdW}}$ ) and electrostatic ( $E_{\text{elect}}$ ) interaction energies. In the bound state, it was assumed that there was only one conformation accessible to each ligand; its conformational entropy is, therefore, zero. In this manner, the binding energy ( $\Delta G_{\text{bind}}$ ) was calculated, as shown in eq 2:

$$\Delta G_{\text{bind}} = \Delta E_{\text{intra}} + \Delta G_{\text{solv}} - T\Delta S_{\text{conf}} + E_{\text{vdW}} + E_{\text{elect}} + E_{\text{ptn}} \quad (2)$$

In eq 2,  $\Delta E_{\text{intra}}$  and  $\Delta G_{\text{solv}}$  are the intramolecular strain and the desolvation penalty for each ligand upon binding. Similarly,  $-T\Delta S_{\text{conf}}$  is the ligand conformational entropy penalty, multiplied by the temperature to convert it into free energy. The final ranking was obtained by calculating relative binding energies ( $\Delta\Delta G_{\text{bind}}$ ) using the top-scoring inhibitor of each target as reference. As mentioned before, in our MM-GB/SA implementation, although solvent effects are included in the protein–ligand complex geometry optimization using GB/SA, the protein desolvation term calculated by the continuum model ( $\Delta G_{\text{solv}}^{\text{ptn}}$ ), defined as illustrated in Figure 3, was excluded from the scoring. This protocol is now fully automated within Knime.<sup>28</sup>

**WaterMap.** In WaterMap, the reference state consists of an assumed-to-preexist cavity in solution formed to accommodate the ligand. In order to allow ligand binding, the binding site waters get displaced to the cavity in solution, leaving a cavity of identical size and shape in the protein (Figure 4). The displaced solvent functional in WaterMap represents an attempt to estimate the free energy liberation ( $\Delta G_{\text{WM}}$ ) for the binding site waters into bulk solution upon cavity transfer between the two environments. This functional depends on the degree of overlap between the ligand heavy atoms and the hydration sites and the energetics of the waters that are displaced. Specifically, the functional considers that a water molecule

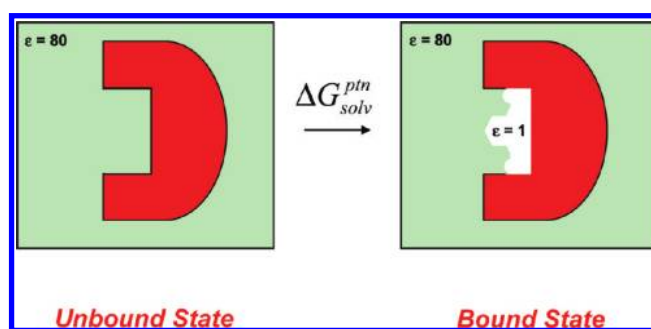
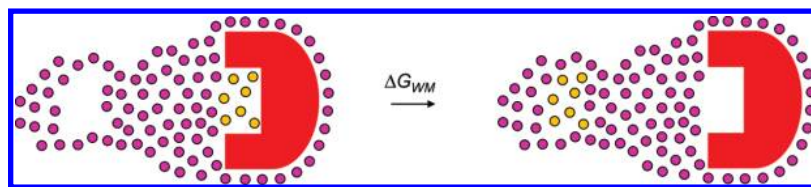


Figure 3. Schematic representation of the protein desolvation term ( $\Delta G_{\text{solv}}^{\text{ptn}}$ ) described by GB/SA. The white area represents the vacuum region in the protein binding site that will be occupied by a ligand of that shape and size.

is completely displaced and, therefore, its full energy is liberated when the distance between the hydration site center and the ligand heavy atom approaches zero. The energy of hydration site displacement then decreases linearly to a value of zero when the distance between the two atoms is equal to 80% of the sum of their vdW radii, beyond which there is no displacement. Multiple ligand atoms may contribute to the displacement of a given hydration site; however, these contributions cease once total displacement is achieved. The ab initio form of the displaced solvent functional, as described by Abel and co-workers, was employed in this work.<sup>21</sup> The thermodynamic and structural properties of theoretical water molecules in the binding sites of factor Xa and CDK2 were obtained from MD simulations of 10 ns each using WaterMap.<sup>29</sup> The protein heavy atoms were harmonically restrained to their starting coordinates.

**FEP Simulations.** Figure 5 illustrates the thermodynamic cycle used to calculate free energy changes.<sup>30</sup> Since free energy is a thermodynamic state function, eq 3 can be derived from the cycle and used to calculate the relative protein–ligand binding free energy ( $\Delta\Delta G_{\text{bind}}$ ), where **A** and **B** are any two analogs,  $\Delta G_{\text{bind}}$  is the absolute binding free energy, and  $\Delta G_{\text{w}}(\mathbf{A} \rightarrow \mathbf{B})$  and  $\Delta G_{\text{p}}(\mathbf{A} \rightarrow \mathbf{B})$  are the free energies associated with the transformation of **A** into



**Figure 4.** Schematic representation of the process simulated by WaterMap. The white area represents the cavity in the bulk that is transferred to the protein binding site. The orange dots represent the binding site waters that get displaced into the bulk solution. WaterMap estimates the free energy liberation ( $\Delta G_{WM}$ ) for the displaced waters.

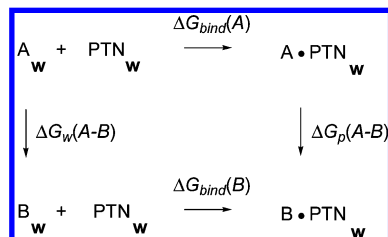


**Figure 5.** Thermodynamic cycle used for the calculation of relative binding free energies ( $\Delta\Delta G_{bind}$ ).  $\Delta G_{bind}$  is the absolute binding free energy.  $\Delta G_w$  and  $\Delta G_p$  are the free energy changes for the transformation of ligand **A** into **B** in water and in the solvated complex.

**B** in water and in the solvated complex, computed by the FEP method.<sup>15–20</sup>

$$\Delta\Delta G_{bind} = \Delta G_{bind}(\mathbf{B}) - \Delta G_{bind}(\mathbf{A}) = \Delta G_p(\mathbf{A} \rightarrow \mathbf{B}) - \Delta G_w(\mathbf{A} \rightarrow \mathbf{B}) \quad (3)$$

FEP simulations were performed for selected pairs of factor Xa inhibitors in Table 3 using the Monte Carlo (MC) sampling technique, as implemented in MCPRO+.<sup>31</sup> Following a series of restrained, partial minimizations using the OPLS\_2005 force field to alleviate bad contacts in the original crystal structure, the degrees of freedom for the protein backbone atoms were not sampled in the MC simulations. The only protein degrees of freedom allowed to vary during the simulation were the bond and dihedral angles for the side chains of residues with any atom within 10 Å from the ligands. The ligands, however, are fully flexible in the MC simulations, except as specified below. Charge neutrality for the protein systems was imposed by assigning normal protonation states at physiological pH to basic and acidic residues near the active site and by making the adjustments for neutrality to the most distant residues. The complexes were solvated with a 22 Å radius water cap. A half-harmonic potential with a force constant of 1.5 kcal/mol·Å<sup>2</sup> was applied to water molecules at distances greater than 22 Å from the center of the system to discourage evaporation. As discussed previously,<sup>32</sup> the use of a spherical cap of water rather than periodic boundary conditions affects the calculated free energies of hydration in simple systems. Therefore, to cancel any potential errors, a 22 Å cap was also used for the **A** → **B** unbound perturbations yielding  $\Delta G_w(\mathbf{A} \rightarrow \mathbf{B})$ .

The **A** → **B** transformations in all environments were performed using the single topology approach by melding the force field parameters for bond lengths and angles, torsions, and nonbonded interactions.<sup>33</sup> In order to keep the number of atoms constant, dummy (DM) atoms were introduced for hydrogens that exist in one state and have no counterpart in the other. Bond lengths for perturbations requiring an atom mutation or annihilation/creation of a hydrogen were not sampled; they were treated as geometrical parameters. Bonds containing a DM atom had an equilibrium

value of 0.3 Å. Shrinking the bond length for DM atoms is a common practice to improve convergence in FEP simulations.<sup>20,33–36</sup> The bond angles involving dummy atoms had the same parameters as their counterparts in the other state. Associated unphysical contributions to the free energy differences cancel in a thermodynamic cycle.<sup>34,36</sup> The MC/FEP calculations for the **A** → **B** transformations were executed at 25 °C using double-wide sampling.<sup>33</sup> Residue-based nonbonded cutoffs of 10 Å were employed in all transformations. The initial and final states were coupled using 20 windows with values for the coupling parameter ( $\lambda$ ) evenly distributed between 0 and 1. Initial relaxation of the solvent was performed for  $5 \times 10^6$  configurations, followed by  $10 \times 10^6$  configurations of full equilibration and  $20 \times 10^6$  configurations of data collection for each window in water or in the protein.

Established procedures including Metropolis and preferential sampling were employed, and statistical uncertainties were obtained from the batch means procedure with batch sizes of  $1 \times 10^6$  configurations.<sup>37</sup> Attempted moves of the ligands in water occurred every 60 configurations, while in the complex, attempted moves of the protein systems and the ligand analogs occurred every 10 and 60 configurations, respectively. The TIP4P model<sup>38</sup> was used for water, and the complexes were represented with the OPLS\_2005 force field.

## RESULTS AND DISCUSSION

**MM-GB/SA Plus WaterMap.** The most accurate way to estimate the polar component of protein solvation in a continuum dielectric environment is by solving the PB equation.<sup>39</sup> Since this method is highly computationally demanding, the GB model, which is based on the PB model but contains several approximations, has become quite popular in computational simulations.<sup>40</sup> However, the increase in speed comes at the cost of accuracy. Although the GB model has been shown to give solvation free energies in agreement with experiment for small molecules,<sup>2,41</sup> the performance of this model for simulations of larger biomolecules is questionable at best.<sup>42</sup> As for the nonpolar components of solvation in GB/SA, i.e., the solvent cavity term and the solute–solvent vdW interactions, they are combined in a single term proportional to the solute surface area. This is based on the linear increase in hydration free energy of *n*-alkanes with chain length. As shown by Gallicchio et al., the empirical parametrization of the nonpolar components of hydration free energies based solely on the solvent accessible surface area is insufficient.<sup>43</sup> In addition, as shown by Pitera and van Gunsteren,<sup>44</sup> favorable vdW dispersion between interior atoms of the solute and the solvent, insignificant for small molecules, is an important effect in the solvation of large solutes, such as biopolymers, and is not well captured in a simple surface-area dependent term. This

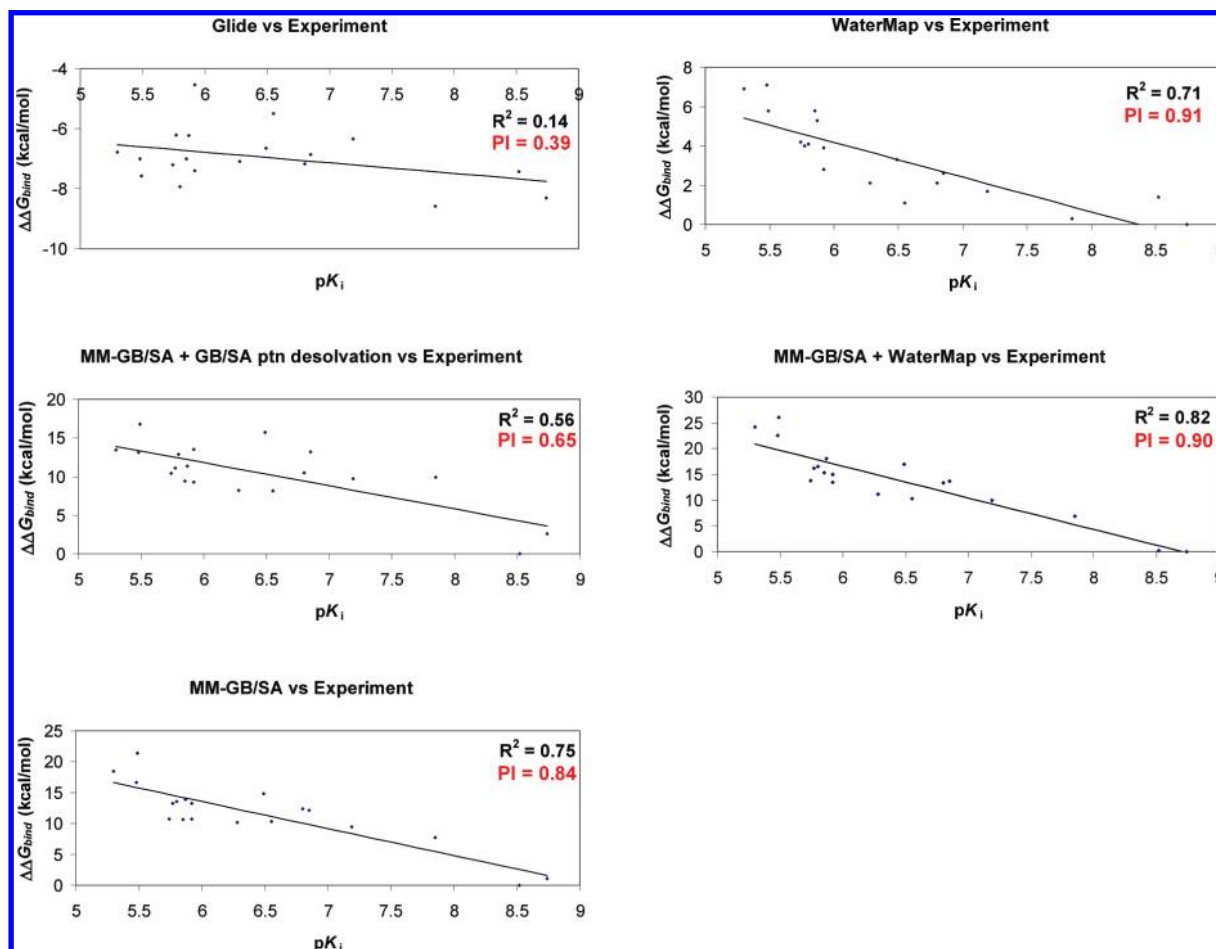


**Figure 6.** Correlation between experimental  $K_i$  values for factor Xa inhibitors and GlideXP, MM-GB/SA, and WaterMap scoring procedures. MM-GB/SA including the GB/SA protein desolvation and the WaterMap free energy liberation are also analyzed. The predictive index (PI) values obtained with each method are shown in red.

is particularly problematic when protein systems differ significantly in the number of buried and solvent-exposed atoms, which is the case when estimating the different protein desolvation contributions caused by each ligand.

Binding poses for the selected factor Xa and CDK2 congeneric series of inhibitors were obtained by Glide. While the poses accurately position the core, there is poor correlation between the Glide XP score and the experimental data for both systems (Figures 6 and 7). Rescoring with the MM-GB/SA method significantly improves correlation with the experiment over docking, with better results when the protein desolvation estimated by the continuum solvation model, calculated as shown in Figure 3, is excluded. This is likely due to the poor description of the polar and/or nonpolar components of solvation for macromolecules described above; the evaluation of which component plays a more important role in decreasing the accuracy of the MM-GB/SA scoring procedure is beyond the scope of this work.

The  $\Delta G_{WM}$  values calculated for the waters displaced by the ligand provide excellent correlations with the experimental data. The  $R^2$  obtained by the WaterMap method alone is 0.71 for factor Xa and 0.68 for CDK2. This indicates that the free energy associated with the hydrophobic effect, estimated by the WaterMap method, accounts for a significant portion of the binding energy differences, at least for congeneric series where other contributions to binding may be somewhat similar for many members of the series.

Interestingly, the MM-GB/SA scoring with no protein desolvation included also performs well with similar  $R^2$  values for factor Xa and CDK2 (0.75 and 0.65, respectively).

Except for the change in surface area for the ligand from the unbound to the bound state in the  $\Delta G_{solv}$  term (Figure 2), the hydrophobic effect is not captured, at least explicitly, by the MM-GB/SA scoring with no protein desolvation included. In addition, the SA component of the ligand  $\Delta G_{solv}$  term is very small compared to the respective GB component and is roughly constant for all members within the individual congeneric series. Thus, it is unlikely that the change in surface area for the ligand represents the hydrophobic effect in the same way WaterMap does and is definitely not the reason for the good results obtained with MM-GB/SA. Hence, WaterMap and MM-GB/SA seem to be describing separate contributions to binding, which happen to correlate well with the experimental data when plotted individually. This implies that their combination should provide the best results.

It should be noted that the SA component of the  $\Delta G_{solv}$  term contains the change in the solvent cavity term for the ligand upon binding; a double counting of effects is then possible since this contribution is supposedly included in  $\Delta G_{WM}$ . However, the solute–solvent vdW interactions and the solvent cavity term are bundled in the SA component. Thus, in theory, eliminating the SA component of the  $\Delta G_{solv}$  term from the scoring to avoid double counting means that the loss of solute–solvent vdW interactions upon binding

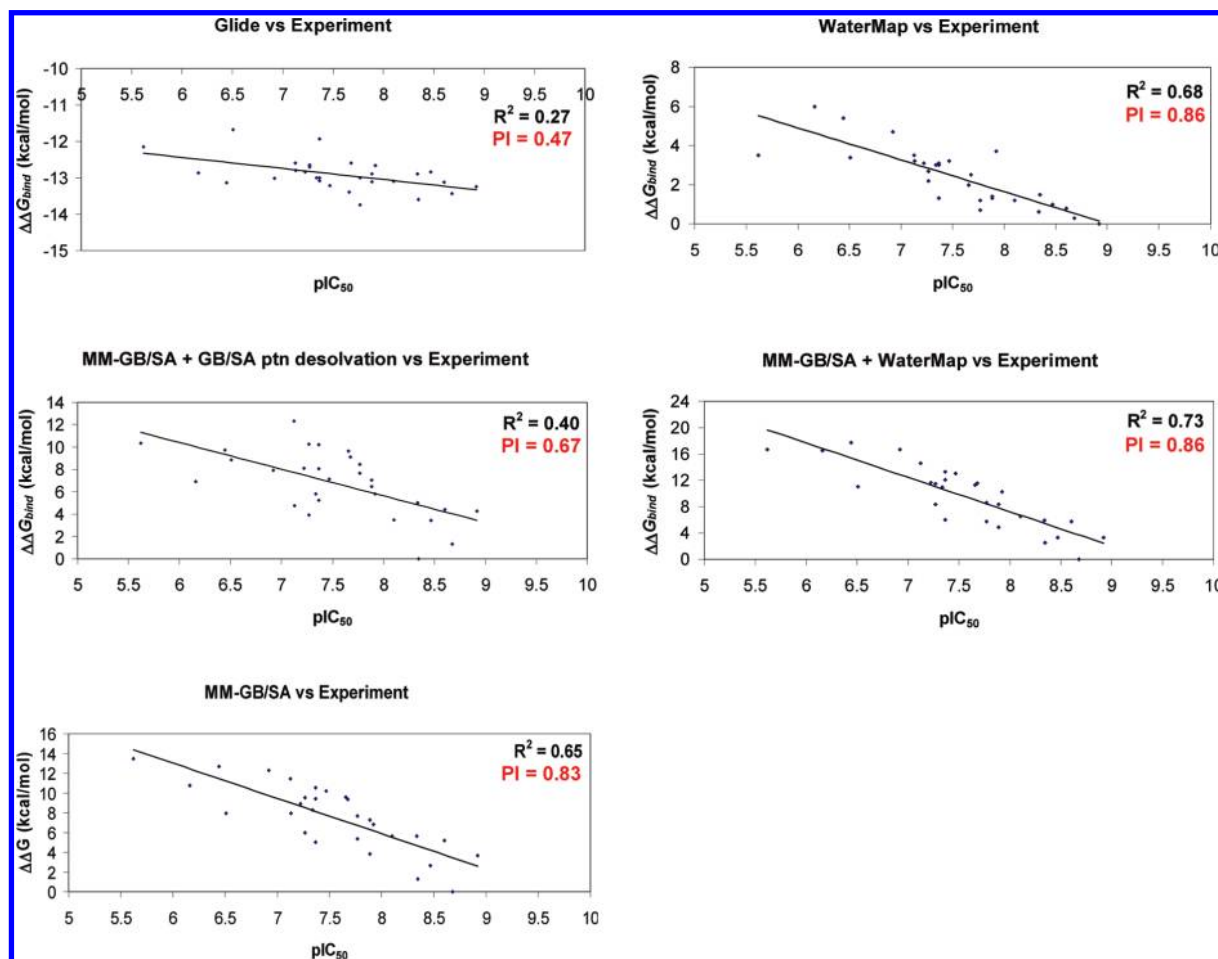


**Figure 7.** Correlation between experimental  $IC_{50}$  values for CDK2 inhibitors and GlideXP, MM-GB/SA, and WaterMap scoring procedures. MM-GB/SA including the GB/SA protein desolvation and the WaterMap free energy liberation are also analyzed. The PI values obtained with each method are shown in red.

would not be taken into account. In practice, since the SA component is irrelevant when compared to the GB component of the  $\Delta G_{solv}$  term, keeping it or not when combining the methods produces essentially the same scores.

The combination of MM-GB/SA and WaterMap indeed gives the best correlation for both targets. However, the improvement in  $R^2$  is modest. Compared to MM-GB/SA with no protein desolvation, for factor Xa  $R^2$  changes from 0.75 to 0.82 and for CDK2 it changes from 0.65 to 0.73. This implies that  $\Delta G_{WM}$  is correlated to the MM-GB/SA term(s) that dominate(s) the binding energy differences. This will be addressed in detail in the next section. Given possible sources of noise in the experiment, one should also consider what would be the realistic upper bound for a “perfect” method. According to Brown and co-workers,<sup>45</sup> an  $R^2$  value of approximately 0.8 is the best a method can do for a data set containing about 30 points, experimental activity covering three orders of magnitude, and having an experimental error of two-fold. Hence, the results obtained by the combined method are almost as good as one can obtain. The quality of the correlations obtained by the combined method as well as by MM-GB/SA and WaterMap individually can also be attested by the  $R^2$  values extracted from the analysis of the experimental data against the ligand molecular weight (MW) and calculated log  $P$  values. For factor Xa  $R^2$  values of 0.35 and 0.34, with a reversed correlation for the latter, were obtained with MW and log  $P$ , respectively, while  $R^2$  values

of 0.13 and 0.02 were obtained for CDK2. These results indicate that physics-based methodologies provide a much more elaborate description of the binding process than a simple estimate of size and hydrophobicity.

Besides  $R^2$  values, the scoring ability of all methods were evaluated using the Predictive Index, PI, introduced by Pearlman and Charifson.<sup>46</sup> The feature of greatest importance in the PI index is not the exact free energies calculated by the method, but rather its reliability in correctly ranking the members of a congeneric series. For a set of experimental  $pK_i$  or  $pIC_{50}$  values,  $E(i)$ , and corresponding predicted scores,  $P(i)$ , the PI index is defined as in eq 4:

$$PI = \frac{\sum_{j>i} \sum_i w_{ij} C_{ij}}{\sum_{j>i} \sum_i w_{ij}} \quad (4)$$

with

$$w_{ij} = |E(j) - E(i)| \quad (5)$$

and

$$C_{ij} = \begin{cases} 1 & \text{if } [E(j) - E(i)]/[P(j) - P(i)] < 0 \\ -1 & \text{if } [E(j) - E(i)]/[P(j) - P(i)] > 0 \\ 0 & \text{if } [P(j) - P(i)] = 0 \end{cases} \quad (6)$$



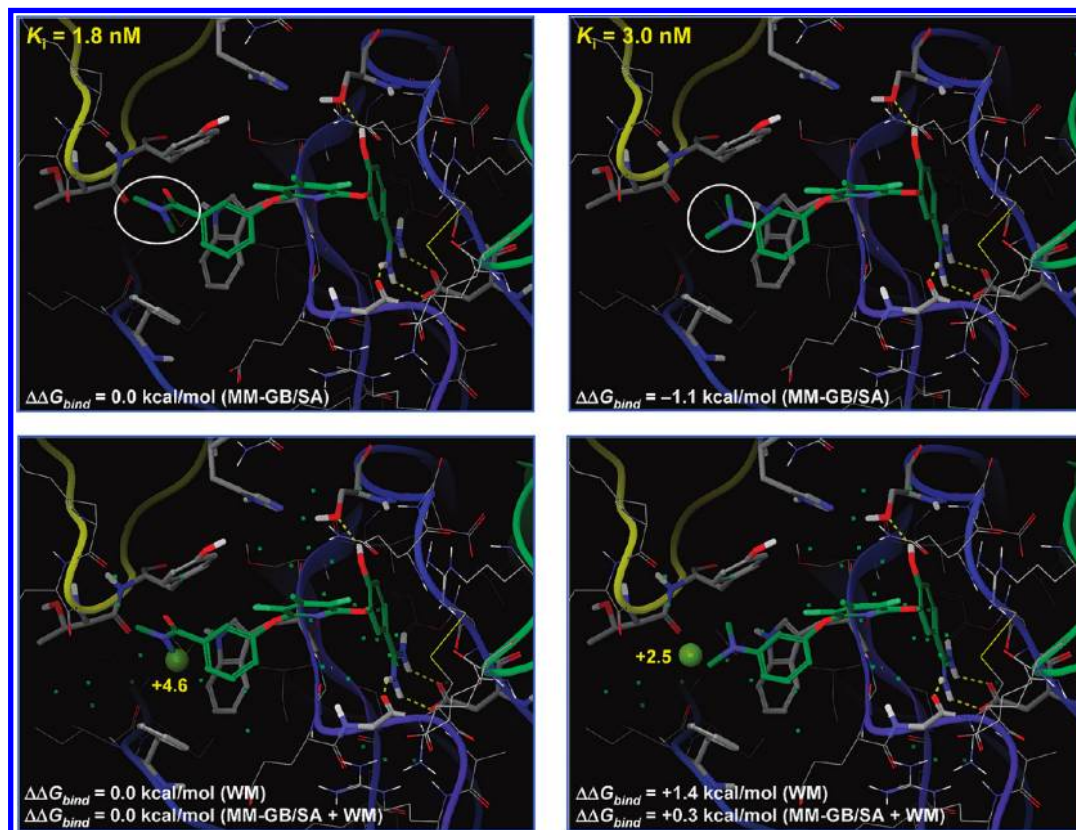


**Figure 8.** Example of improvement obtained with the MM-GB/SA and the WaterMap (WM) combination for a pair of factor Xa inhibitors. Free energies for key hydration sites with respect to bulk water are also shown (values in kcal/mol).

The index ranges from  $-1$  to  $+1$ , depending on how well the predictions track the experimental rank order, with  $+1$  for perfect prediction,  $-1$  for predictions that are always wrong, and  $0$  for completely random predictions. It should be noted that this function includes a weighting term that depends on the difference between the experimental values. A good function should be able to differentiate between changes that result in large differences in the experimental binding affinity.

Figures 6 and 7 show the PI values obtained by each method when ranking the congeneric series of factor Xa and CDK2 inhibitors. They display a very similar picture to the one obtained by the analysis of the  $R^2$  values. The Glide XP score has the worst PI values followed by the MM-GB/SA method including the protein desolvation estimated by the continuum solvation model. MM-GB/SA with no protein desolvation included performs very well with a slight improvement upon combination with WaterMap. Interestingly, the WaterMap free energy liberation alone has the best PI values. This might be related to the fact that the MM-GB/SA scoring equation is a sum of many terms and is more subject to inaccuracies in the energy function, the force field and the GB/SA method used, that can lead to few shifts in the predicted rank order with respect to the experimental one.

As discussed above, the incorporation of  $\Delta G_{WM}$  into the MM-GB/SA method improves the  $R^2$  and PI values. Specifically, their combination corrects the rank order of a few pairs of ligands incorrectly ranked by the MM-GB/SA method alone, like the one illustrated in Figure 8 for factor Xa. According to MM-GB/SA, the ligand with the amino group binds more favorably than the one with the amide by  $-1.1$  kcal/mol, while WaterMap predicts a more unfavorable binding for the former by  $+1.4$  kcal/mol since the waters it

displaces are not so unfavorable. The score combination then predicts that the amino group binds less favorably than the amide by  $+0.3$  kcal/mol, which agrees with the experimental difference in  $K_i$  values,  $3.0$  nM for the amino and  $1.8$  nM for the amide (i.e.,  $+0.3$  kcal/mol).

**MM-GB/SA Versus WaterMap.** As mentioned above, the WaterMap method alone provides an excellent correlation with the experimental data for both targets. MM-GB/SA with protein desolvation excluded also performs very well, with similar  $R^2$  and PI values as the ones obtained with WaterMap. Their combination would potentially result in the best agreement with the experiment since WaterMap and MM-GB/SA are theoretically describing different contributions to binding, the hydrophobic effect in the former and mainly the loss of ligand–solvent interactions, the gain of protein–ligand interactions, and the resultant strain upon binding in the latter. The improvement in  $R^2$  and PI values, however, is modest when both are combined. As discussed above, this might be due to the fact that the combined method is approaching the maximum  $R^2$  value a model can obtain given the properties of the data sets studied. The small improvement can also be explained by the high correlation between the free energy liberation estimated by WaterMap and by the MM-GB/SA scoring approach; when comparing the methods  $R^2$  values of  $0.61$  and  $0.57$  are obtained for CDK2 and factor Xa, respectively.

Obviously, WaterMap has no information regarding MM-GB/SA ligand-based contributions, such as the loss of ligand–solvent interactions, the intramolecular strain, and the conformational entropy penalties. The displaced solvent functional also does not have any information about the protein strain induced by the different ligands, as the WaterMap scoring is



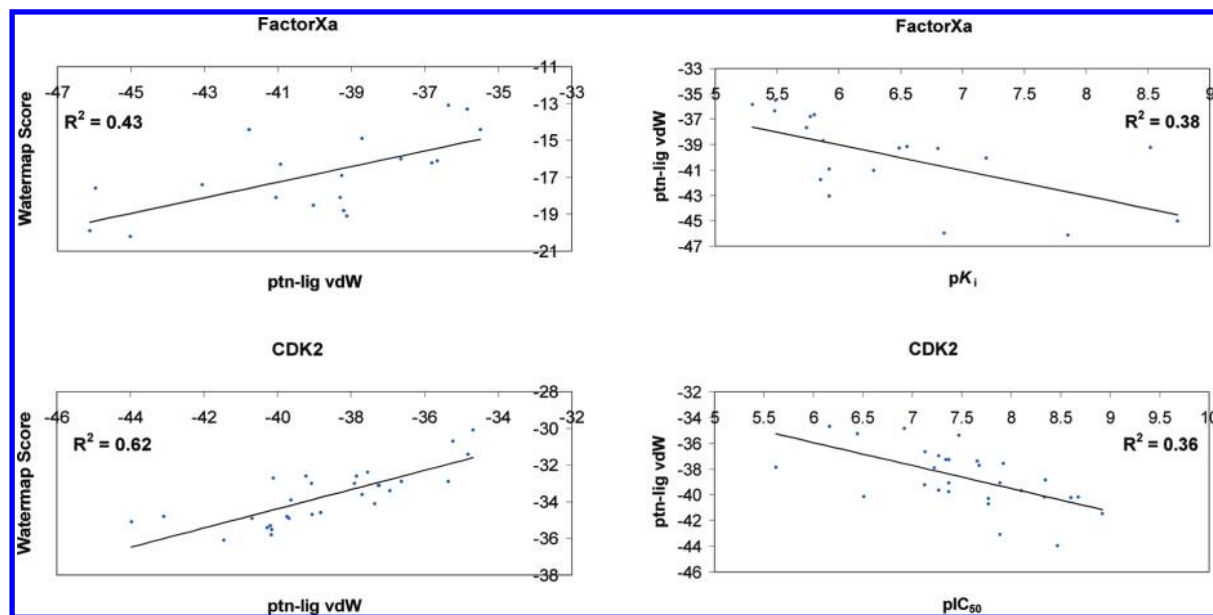


**Figure 9.** Correlation between protein–ligand vdW interactions and WaterMap free energy liberation values (left). The protein–ligand vdW interaction term is the one that dominates the binding energy differences (right).

performed using the same protein conformation for all of them. Finally, protein–ligand electrostatic interactions are not taken into account because the WaterMap functional is equally affected if a given binding site water is displaced by a polar or nonpolar ligand atom. The only MM-GB/SA term left is the protein–ligand vdW interactions.

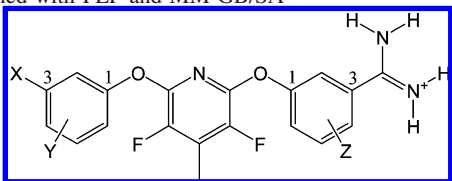
As can be seen in Figure 9, the high correlation between the WaterMap and MM-GB/SA results has its origin in the significant correlation between the protein–ligand vdW interactions and the WaterMap  $\Delta G_{WM}$  values. This should be expected since ligands that engage in more favorable vdW interactions with the protein, provided they do not sterically clash with binding site residues, tend to be larger and, consequently, displace more binding site waters. Since most waters in the factor Xa and CDK2 binding sites are unfavorable with respect to bulk solution, as more of them get displaced, the WaterMap free energy liberation becomes more favorable. Obviously, size is an important aspect but not enough to fully explain the correlation between the protein–ligand vdW interactions and the WaterMap  $\Delta G_{WM}$  values. Perhaps more important than the quantity of water molecules is the specific binding site thermodynamic properties of the ones that get displaced. In this case, the correlation can be explained by the good fit between the protein and the ligand that optimally places nonpolar groups in the most hydrophobic pockets, which typically contain the most unfavorable water molecules. Ligands that accomplish that, regardless of their size, should not only engage in more favorable vdW interactions but also display more negative WaterMap  $\Delta G_{WM}$  values. In retrospective analyses for congeneric series containing only active ligands, like the ones evaluated in this work, the correlation between the WaterMap  $\Delta G_{WM}$  values and the protein–ligand vdW interactions will probably always exist. One possible exception is for regions that exhibit hydrophobic enclosures, i.e., are surrounded by hydrophobic protein atoms. They provide a much less favorable environment for water molecules that would result in much more favorable  $\Delta G_{WM}$  values upon water displacement than reflected in the protein–ligand vdW interactions.<sup>21a</sup> Another possible exception is when comparing ligands in prospective

design, the designed analogs may have severe steric clashes with the protein but very favorable  $\Delta G_{WM}$  values due to the thermodynamics and the number of waters that they displace.

The good agreement with the experimental data obtained by WaterMap suggests that the binding energy differences for the two congeneric series are dominated by the hydrophobic effect. MM-GB/SA also performs well because this effect is captured, to some extent, by the protein–ligand vdW interactions term. For both factor Xa and CDK2, the protein–ligand vdW interaction term, out of all MM-GB/SA contributions, is the one that dominates the binding energy differences (Figure 9). It should be noted that the other MM-GB/SA terms do contribute as their inclusion in the score greatly improves the correlation with the experimental data when compared to protein–ligand vdW interactions alone (Figures 6 and 7).

Although the WaterMap method works well for both congeneric series, the results obtained here should not be generalized. For example, it is likely that WaterMap will struggle when the binding process is dominated by some other contribution, such as protein–ligand electrostatic interactions or ligand-based terms, e.g., intramolecular strain and desolvation penalty. For comparisons between chemical series, both methods will likely perform poorly due to the importance of other contributions to binding, mostly entropic, not contemplated by either WaterMap or MM-GB/SA, by different protein conformational changes induced by diverse scaffolds, and by the lack of cancellation of errors in the empirical energy function.

**Large Dynamic Range in MM-GB/SA: Comparison with FEP results.** Figures 6 and 7 show a large dynamic range for the MM-GB/SA score with no protein desolvation when compared to the experimental range. The inclusion of the GB/SA protein desolvation partially attenuates this problem; in GB/SA, a more unfavorable protein desolvation due to a more pronounced loss of protein–solvent electrostatic interactions is generally obtained for more active ligands because they tend to fill more of the pocket. The combination of the WaterMap  $\Delta G_{WM}$  values and the MM-

**Table 4.** Relative Binding Free Energies Obtained with FEP and MM-GB/SA<sup>a</sup>


XA	XB	Y	ZA	ZB	$\Delta\Delta G_{\text{bind}}$ exp	$\Delta\Delta G_{\text{bind}}$ FEP	$\Delta\Delta G_{\text{bind}}$ MM-GB/SA	$\Delta\Delta G_{\text{bind}}$ MM-GB/SA (RRHO) <sup>b</sup>	$\Delta\Delta E_{\text{elect}}$ MM-GB/SA <sup>c</sup>
N(CH <sub>3</sub> ) <sub>2</sub>	N(CH <sub>3</sub> ) <sub>2</sub>	H	<i>6-CH<sub>3</sub></i>	<i>6-OH</i>	-3.6	-3.5	-10.7	-10.8	-18.5
N(CH <sub>3</sub> ) <sub>2</sub>	N(CH <sub>3</sub> ) <sub>2</sub>	H	<i>H</i>	<i>6-OH</i>	-2.4	+0.2	-12.4	-12.3	-31.1
N(CH <sub>3</sub> ) <sub>2</sub>	N(CH <sub>3</sub> ) <sub>2</sub>	H	<i>6-NH<sub>2</sub></i>	<i>6-OH</i>	-1.8	-1.9	-9.4	-9.5	-12.9
<i>NH<sub>2</sub></i>	<i>N(CH<sub>3</sub>)<sub>2</sub></i>	H	H	H	-1.8	-3.8	-4.2	-3.9	+4.2
<i>OCH<sub>3</sub></i>	<i>N(CH<sub>3</sub>)<sub>2</sub></i>	H	H	H	-1.3	-1.2	-1.5	-0.9	+0.4
<i>COCH<sub>3</sub></i>	<i>N(CH<sub>3</sub>)<sub>2</sub></i>	H	H	H	-1.3	+3.0	+1.8	+1.8	+0.5

<sup>a</sup> Only perturbations for the X and Z substituents were performed using the FEP method. The specific mutations are shown in italic.

<sup>b</sup> MM-GB/SA relative binding free energies, including entropic contributions obtained using the RRHO approximation. These entropic contributions exclude vibrational contributions from torsional motions. <sup>c</sup> Change in protein–ligand electrostatic interactions for a pair of ligands according to MM-GB/SA.

GB/SA score excluding the GB/SA protein desolvation accentuates the already large dynamic range due to the direct correlation between the protein–ligand vdW interactions and the WaterMap  $\Delta G_{\text{WM}}$  values. Although not evaluated in this work, it is possible that the simple combination of the two methods could result in an unbalance of the contributions to binding that would lead to a score that preferentially selects more hydrophobic molecules in prospective drug design over smaller and more polar compounds that engage in productive hydrogen bonds with the receptor.

The large dynamic range observed in the MM-GB/SA scoring could also have its origin in other effects. For example, it is possible that the wider scoring spread is due to the application of a protein dielectric constant of 1 in a model where protein motions and polarization are not taken into account. In this case, electrostatic interactions are not shielded enough, and protein–ligand electrostatic attractions and repulsions are overestimated, causing the large separation of potent and weak compounds. Another potential explanation is associated with the incomplete description of enthalpy–entropy compensation; only the conformational entropy penalty for the ligand upon binding is included. Since translational, rotational, and vibrational entropy changes are ignored, the ligands that interact the most favorably with the protein are not entropically penalized due to restriction of their vibrational modes in the binding site. Also, the ligands with higher molecular weight that tend to display a more favorable hydrophobic effect and vdW interactions are not penalized due to greater loss of translational and rotational entropies upon binding; the rigid-body entropy of a free molecule in solution has a logarithmic dependence on its molecular weight.<sup>47</sup> Another important entropic contribution is associated with the narrowing of the torsional energy wells for the ligands when in the protein environment compared to solution. More flexible ligands, which have the opportunity to maximize their interactions with the protein, should pay a more significant vibrational entropy penalty due to restriction of their torsional motions.<sup>48</sup>

Considered the reference technique, FEP simulations were run for selected pairs of factor Xa inhibitors to shed some light in the origin of the large dynamic range provided by the MM-GB/SA score. When comparing the results, one should

be aware of the particularities of each approach that can lead to some of the discrepancies in the free energy values that are not necessarily related to the different methodologies. To minimize part of this problem, OPLS\_2005 was used for both FEP and MM-GB/SA calculations. However, since FEP simulations cannot be run using GB/SA in MCPRO+, the explicit TIP4P solvation model was used.

Another important aspect is that, although the FEP equation is exact, the simulation length and the sampled degrees of freedom both have great impact on the accuracy of the FEP results. In MCPRO+, only the side chains of residues with any atom within 10 Å from the ligands were varied; the protein backbone is fixed. Although the ligand is free to move in the unbound state, one should not expect that all the accessible conformations and the full range of dihedral angle values for each torsional energy well are visited, even for very long simulations. This implies that the FEP results will not include all entropic contributions.

Six pairs of ligands were analyzed. The first three in Table 4 involve perturbations where a hydrogen bond between the ligand and the catalytic Ser residue is either lost or changed. Specifically, they include the perturbations of the Z substituent at the 6-position on the benzamidine ring from CH<sub>3</sub>, hydrogen, and NH<sub>2</sub> to OH. The other three pairs involve perturbations in a hydrophobic pocket formed by Phe, Trp, and Tyr residues, one of each (Figure 10). The X substituent on the terminal phenyl group was mutated from NH<sub>2</sub>, OCH<sub>3</sub>, and COCH<sub>3</sub> to N(CH<sub>3</sub>)<sub>2</sub>. The FEP results have very good agreement with the experiment for three pairs, the right trend for one case and the reverse order for two of them. Although correct orders are obtained by the MM-GB/SA scoring for comparisons involving Z = OH, the method overpredicts its binding free energy. Inclusion of rotational, translational, and vibrational entropy changes upon binding using the rigid-rotor harmonic oscillator (RRHO) approximation calculated by MacroModel<sup>27</sup> has no significant impact on the MM-GB/SA results (Table 4); the RRHO correction slightly opposes binding for ligands with higher molecular weight. As for the vibrational contributions, it is possible that the vibrational entropy changes in all cases are similar because they are dominated by the strong salt bridge between the Asp residue in the S1 pocket and the amidine group, present in all ligands

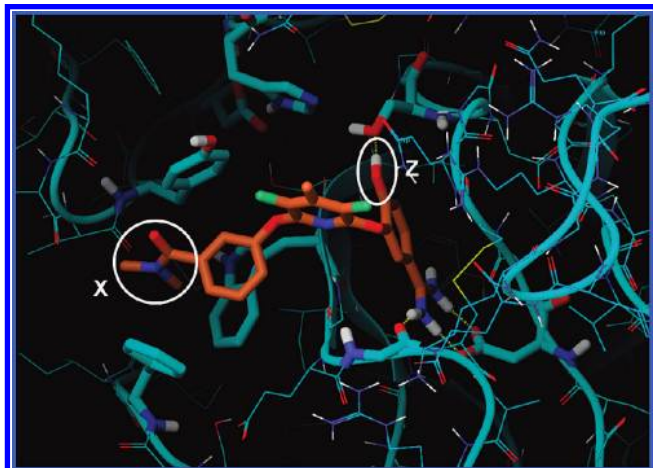


**Figure 10.** Binding pockets where comparisons between functional groups have been performed using FEP and MM-GB/SA are highlighted for a factor Xa inhibitor.

(Figure 10). Thus, the formation of an additional hydrogen bond with the protein would play a minor role. It should be noted that due to the high computational cost, the entropic contributions exclude vibrational contributions from torsional motions. However, lack of an entropic penalty originated in the narrowing of the torsional energy well for the dihedral angle connecting the OH group and the phenyl ring upon binding is unlikely to be the cause for the large separation; this energy well is already significantly narrow in the unbound state due to conjugation effects. The same argument is valid for the mutations involving the X substituents due to conjugation with the terminal phenyl ring.

Analysis of the MM-GB/SA scoring terms revealed that the overly favorable protein–ligand electrostatic interactions between the OH group and the Ser residue are the origin of the problem here. This is supported by the good agreement between the FEP and MM-GB/SA results for the pairs of ligands with changes of functional groups in a hydrophobic pocket where no intermolecular hydrogen bonds are present. Table 4 shows that the change in protein–ligand electrostatic interactions is not exaggerated in those cases. Although the pairs of ligands selected do not address the impact of the incomplete description of enthalpy–entropy compensation effects in MM-GB/SA scoring due to the nature of the mutations studied, they clearly highlight the importance of the appropriate treatment of protein–ligand electrostatic interactions. In the case of factor Xa, the lack of shielding effects of protein–ligand electrostatic interactions did not affect the correlation with experiment because the hydrogen bond between the ligand and the protein provided a boost in potency. This is not always true. There are many examples of hydrogen bonds that result in either no gain or a drop in potency because of increased ligand desolvation penalty. For the MM-GB/SA technique to be useful in the prospective design of compounds that engage in hydrogen bonds with the receptor, it is crucial that the score provide the correct balance between the ligand desolvation penalty and the electrostatic interactions with the protein.

## CONCLUSIONS

In this work, we investigated the impact caused by poor estimation of protein desolvation by the GB/SA solvation

model and the large dynamic range observed in the MM-GB/SA scoring compared to the experimental range. In the former, the exclusion of the GB/SA protein desolvation term from the MM-GB/SA scoring significantly improves correlation with the experiment when ranking congeneric series of factor Xa and CDK2 inhibitors. This is probably due to poor description by the GB/SA continuum solvation model of the underlying physics involved in the solvation of complex systems, such as proteins. The changes in protein–solvent electrostatic interactions, solvent cavity, and protein–solvent vdW interactions upon protein desolvation are likely not well captured by the approximations used in the GB model and by the simple difference in surface area between the protein bound and unbound states.

The best results were provided by the incorporation of the WaterMap free energy liberation of binding site waters into the MM-GB/SA scoring procedure that excludes the GB/SA protein desolvation. In spite of that, the improvement was modest over results obtained with the MM-GB/SA and WaterMap methods individually. It is possible that part of the small improvement is due to the fact that the combined method is approaching the maximum  $R^2$  value a model can obtain given the properties of the data sets studied, as suggested by Brown and co-workers.<sup>45</sup> The small improvement can also be explained by the high correlation between the WaterMap free energy liberation and the term that computes protein–ligand vdW interactions in MM-GB/SA scoring; the former is a measure of the hydrophobic effect and the latter of hydrophobic-like interactions. Specifically, ligands that engage in more favorable vdW interactions with the protein tend to be either larger or place nonpolar groups more optimally into the most hydrophobic pockets. Consequently, they displace more unfavorable waters from the protein binding sites, resulting in a more favorable WaterMap free energy liberation.

As for the large dynamic range, the wider MM-GB/SA scoring spread might be due to the application of a protein dielectric constant of 1 in a model where protein motions and polarization are not taken into account and/or associated with the incomplete description of enthalpy–entropy compensation effects. Comparisons between MM-GB/SA and FEP calculations point to the former for the factor Xa test set; the lack of shielding effects of protein–ligand electrostatic interactions overly favors the ligands that engage in hydrogen bonds with the protein. Although the pairs of ligands selected do not address the incomplete description of enthalpy–entropy compensation effects, they clearly highlight the importance of the appropriate treatment of protein–ligand electrostatic interactions.

Finally, although not investigated in this work, it is conceivable that the simple combination of the two methods could result in an unbalance of the energetics that would lead to a score that preferentially selects more hydrophobic molecules in prospective drug design over smaller and more polar compounds that engage in productive hydrogen bonds with the receptor. On the other hand, since it is also apparent from the FEP calculations that the electrostatic contribution to binding in the MM-GBSA calculations is overweighted due to the lack of dynamical screening effects, it may be possible that our combined model has a roughly correct balance of hydrophobic and polar contributions, albeit with too large of a slope. However, for the MM-GB/SA technique



to be useful in cases where the binding process is mainly dominated by electrostatic effects, such as those for congeneric series containing ligands with similar size and shape but differing in their charge distributions, it is crucial that the score provides the correct balance between the ligand desolvation penalty and the electrostatic interactions with the protein. This will be the subject of future research.

#### ACKNOWLEDGMENT

The authors would like to thank Woody Sherman and Robert Abel from Schrodinger, Inc., for carefully reading the manuscript and for providing invaluable suggestions. Gratitude is also expressed to Gabriela Barreiro for helpful discussions.

**Supporting Information Available:** Files containing the protein coordinates, locations for the binding site waters, ligand poses, and the Watermap scores are provided. The thermodynamic data obtained by Watermap is included in Microsoft Excel files. This information is available free of charge via the Internet at <http://pubs.acs.org/>.

#### REFERENCES AND NOTES

- (1) (a) Kuhn, B.; Kollman, P. A. Binding of a Diverse Set of Ligands to Avidin and Streptavidin: An Accurate Quantitative Prediction of their Relative Affinities by a Combination of Molecular Mechanics and Continuum Solvent Models. *J. Med. Chem.* **2000**, *43*, 3786–3791. (b) Baril, X.; Gelpi, J. L.; López, J. M.; Orozco, M.; Luque, F. J. How Accurate Can Molecular Dynamics/Linear Response and Poisson-Boltzmann/Solvent Accessible Surface Calculations Be for Predicting Relative Binding Affinities? Acetylcholinesterase Huiprine Inhibitors as a Test Case. *Theor. Chem. Acc.* **2001**, *106*, 2–9.
- (2) Still, W. C.; Tempczyk, A.; Hawley, R. C.; Hendrickson, T. Semi-analytical Treatment of Solvation for Molecular Mechanics and Dynamics. *J. Am. Chem. Soc.* **1990**, *112*, 6127–6129.
- (3) Kuntz, I. D.; Blaney, J. M.; Oatley, S. J.; Langridge, R.; Ferrin, T. E. A Geometric Approach to Macromolecule-Ligand Interactions. *J. Mol. Biol.* **1982**, *161*, 269–288.
- (4) Jones, G.; Willet, P.; Glen, R. C.; Leach, A. R.; Taylor, R. Development and Validation of a Genetic Algorithm for Flexible Docking. *J. Mol. Biol.* **1997**, *267*, 727–748.
- (5) Rarey, M.; Kramer, B.; Lengauer, T.; Klebe, G. A Fast Flexible Docking Method using an Incremental Construction Algorithm. *J. Mol. Biol.* **1996**, *261*, 470–489.
- (6) Friesner, R. A.; Banks, J. L.; Murphy, R. B.; Halgren, T. A.; Klicic, J. J.; Mainz, D. T.; Repasky, M. P.; Knoll, E. H.; Shelley, M.; Perry, J. K.; Shaw, D. E.; Francis, P.; Shenkin, P. S. Glide: A New Approach for Rapid, Accurate Docking and Scoring. 1. Method and Assessment of Docking Accuracy. *J. Med. Chem.* **2004**, *47*, 1739–1749.
- (7) Muegge, I.; Martin, Y. C. A General and Fast Scoring Function for Protein-Ligand Interactions: A Simplified Potential Approach. *J. Med. Chem.* **1999**, *42*, 791–804.
- (8) Charifson, P. S.; Corkey, J. J.; Murcko, M. A.; Walters, W. P. Consensus Scoring: A Method for Obtaining Improved Hit Rates from Docking Databases of Three-Dimensional Structures into Proteins. *J. Med. Chem.* **1999**, *42*, 5100–5109.
- (9) Perola, E.; Walters, W. P.; Charifson, P. S. A Detailed Comparison of Current Docking and Scoring Methods on Systems of Pharmaceutical Relevance. *Proteins* **2004**, *56*, 235–249.
- (10) Stahl, M.; Rarey, M. Detailed Analysis of Scoring Functions for Virtual Screening. *J. Med. Chem.* **2001**, *44*, 1035–1042.
- (11) Warren, G. L.; Andrews, C. W.; Capelli, A.-M.; Clarke, B.; LaLonde, J.; Lambert, M. H.; Lindvall, M.; Nevins, N.; Semus, S. F.; Senger, S.; Tedesco, G.; Wall, I. D.; Woolven, J. M.; Peishoff, C. E.; Head, M. S. A Critical Assessment of Docking Programs and Scoring Functions. *J. Med. Chem.* **2006**, *49*, 5912–5931.
- (12) Tirado-Rives, J.; Jorgensen, W. L. Contribution of Conformer Focusing to the Uncertainty in Predicting Free Energies for Protein-Ligand Binding. *J. Med. Chem.* **2006**, *49*, 5880–5884.
- (13) (a) Bernacki, K.; Kalyanaraman, C.; Jacobson, M. P. Virtual Ligand Screening against Escherichia coli Dihydrofolate Reductase: Improving Docking Enrichment Physics-Based Methods. *J. Biomol. Screening* **2005**, *10*, 675–681. (b) Huang, N.; Kalyanaraman, C.; Irwin, J. J.; Jacobson, M. P. Physics-Based Scoring of Protein-Ligand Complexes: Enrichment of Known Inhibitors in Large-Scale Virtual Screening. *J. Chem. Inf. Model.* **2006**, *46*, 243–253. (c) Huang, N.; Kalyanaraman, C.; Bernacki, K.; Jacobson, M. P. Molecular Mechanics Methods for Predicting Protein-Ligand Binding. *Phys. Chem. Chem. Phys.* **2006**, *8*, 5166–5177. (d) Lyne, P. D.; Lamb, M. L.; Saeh, J. C. Accurate Prediction of the Relative Potencies of Members of a Series of Kinase Inhibitors using Molecular Docking and MM-GBSA Scoring. *J. Med. Chem.* **2006**, *49*, 4805–4808. (e) Lee, M. R.; Sun, Y. Improving Docking Accuracy through Molecular Mechanics Generalized Born Optimization and Scoring. *J. Chem. Theory Comput.* **2007**, *3*, 1106–1119. (f) Huang, N.; Jacobson, M. P. Physics-Based Methods for Studying Protein-Ligand Interactions. *Curr. Opin. Drug Discovery Dev.* **2007**, *10*, 325–331. (g) Foloppe, N.; Hubbard, R. Towards Predictive Ligand Design with Free-Energy Based Computational Methods. *Curr. Med. Chem.* **2006**, *13*, 3583–3608. (h) Guimarães, C. R. W.; Cardozo, M. MM-GB/SA Rescoring of Docking Poses in Structure-Based Lead Optimization. *J. Chem. Inf. Model.* **2008**, *48*, 958–970. (i) Pearlman, D. A. Evaluating the Molecular Mechanics Poisson-Boltzmann Surface Area Free Energy Method using a Congeneric Series of Ligands to p38 MAP Kinase. *J. Med. Chem.* **2005**, *48*, 7796–807. (j) Kawatkar, S.; Wang, H.; Czerminski, R.; Joseph-McCarthy, D. Virtual Fragment Screening: An Exploration of Various Docking and Scoring Protocols for Fragments using Glide. *J. Comput.-Aided Mol. Des.* **2009**, *23*, 527–539.
- (14) Friesner, R. A.; Murphy, R. B.; Repasky, M. P.; Frye, L. L.; Greenwood, J. R.; Halgren, T. A.; Sanschagrin, P. C.; Mainz, D. T. Extra Precision Glide: Docking and Scoring Incorporating a Model of Hydrophobic Enclosure for Protein-Ligand Complexes. *J. Med. Chem.* **2006**, *49*, 6177–6196.
- (15) Jorgensen, W. L. Free energy changes in solution. In *Encyclopedia of Computational Chemistry*; Schleyer, P. v. R., Ed.; Wiley: New York, 1998; Vol. 2, pp 1061–1070.
- (16) Kollman, P. A. Free Energy Calculations: Applications to Chemical and Biochemical Phenomena. *Chem. Rev.* **1993**, *93*, 2395–2417.
- (17) Jorgensen, W. L. Free Energy Calculations: A Breakthrough for Modeling Organic Chemistry in Solution. *Acc. Chem. Res.* **1989**, *22*, 184–189.
- (18) Simonson, T.; Georgios, A.; Karplus, M. Free Energy Simulations Come of Age: Protein-Ligand Recognition. *Acc. Chem. Res.* **2002**, *35*, 430–437.
- (19) Pearlman, D. A.; Charifson, P. S. Are Free Energy Calculations Useful in Practice? A Comparison with Rapid Scoring Functions for the p38 MAP Kinase Protein System. *J. Med. Chem.* **2001**, *44*, 3417–3423.
- (20) Guimarães, C. R. W.; Boger, D. L.; Jorgensen, W. L. Elucidation of Fatty Acid Amide Hydrolase Inhibition by Potent  $\alpha$ -ketoheterocycle Derivatives from Monte Carlo Simulations. *J. Am. Chem. Soc.* **2005**, *127*, 17377–17384.
- (21) (a) Wade, R. C.; Mazar, M. H.; McCammon, J. A.; Quiocho, F. A. Hydration of Cavities in Proteins: A Molecular Dynamics Approach. *J. Am. Chem. Soc.* **1990**, *112*, 7057–7059. (b) Gilson, M. K.; Given, J. A.; Bush, B. L.; McCammon, J. A. The Statistical-Thermodynamic Basis for Computation of Binding Affinities: A Critical Review. *Biophys. J.* **1997**, *72*, 1047–1069. (c) Hamelberg, D.; McCammon, J. A. Standard Free Energy of Releasing a Localized Water Molecule from the Binding Pockets of Proteins: Double-Decoupling Method. *J. Am. Chem. Soc.* **2004**, *126*, 7683–7689. (d) Zhang, L.; Hermans, J. Hydrophilicity of Cavities in Proteins. *Proteins* **1996**, *24*, 433–438. (e) Barillari, C.; Taylor, J.; Viner, R.; Essex, J. W. Classification of Water Molecules in Protein Binding Sites. *J. Am. Chem. Soc.* **2007**, *129*, 2577–2587. (f) Michel, J.; Tirado-Rives, J.; Jorgensen, W. L. Prediction of the Water Content in Protein Binding Sites. *J. Phys. Chem. B* **2009**, *113*, 13337–13346. (g) Abel, R.; Young, T.; Farid, R.; Berne, B. J.; Friesner, R. A. Role of the Active-Site Solvent in the Thermodynamics of factor Xa Ligand Binding. *J. Am. Chem. Soc.* **2008**, *130*, 2817–2831. (h) Beuming, T.; Farid, R.; Sherman, W. High-energy water sites determine peptide binding affinity and specificity of PDZ domains. *Protein Sci.* **2009**, *18*, 1609–1619. (i) Clausen, R. P.; Naur, P.; Kristensen, A. S.; Greenwood, J. R.; Strange, M.; Brauner-Osborne, H.; Jensen, A. A.; Nielsen, A. S. T.; Genser, U.; Ringgaard, L. M.; Nielsen, B.; Pickering, D. S.; Brehm, L.; Gajhede, M.; Krogsgaard-Larsen, P.; Kastrup, J. S. The Glutamate Receptor GluR5 Agonist (S)-2-Amino-3-(3-hydroxy-7,8-dihydro-6H-cyclohepta[d]-isoxazol-4-yl)propionic Acid and the 8-Methyl Analogue: Synthesis, Molecular Pharmacology, and Biostructural Characterization. *J. Med. Chem.* **2009**, *52*, 4911–4922.
- (22) Bramson, H. N.; Corona, J.; Davis, S. T.; Dickerson, S. H.; Edelstein, M.; Frye, S. V.; Gampe, R. T.; Harris, J. P. A.; Hassell, A.; Holmes, W. D.; Hunter, R. N.; Lackey, K. E.; Lovejoy, B.; Luzzio, M. J.; Montana, V.; Rocque, W. J.; Rusnak, D.; Shewchuk, L.; Veal, J. M.; Walker, D. H.; Kuyper, L. F. Oxindole-Based Inhibitors of Cyclin-Dependent Kinase 2 (CDK2): Design, Synthesis, Enzymatic activities, and X-ray Crystallographic Analysis. *J. Med. Chem.* **2001**, *44*, 4339–4358.

- (23) (a) Phillips, G.; Davey, D. D.; Eagen, K. A.; Koovakkat, S. K.; Liang, A.; Ng, H. P.; Pinkerton, M.; Trinh, L.; Whitlow, M.; Beatty, A. M.; Morrissey, M. M. Design, Synthesis, and Activity of 2,6-diphenoxypyridine-derived factor Xa Inhibitors. *J. Med. Chem.* **1999**, *42*, 1749–1756. (b) Phillips, G.; Guilford, W. J.; Buckman, B. O.; Davey, D. D.; Eagen, K. A.; Koovakkat, S.; Liang, A.; McCarrick, M.; Mohan, R.; Ng, H. P.; Pinkerton, M.; Subramanyam, B.; Ho, E.; Trinh, L.; Whitlow, M.; Wu, S.; Xu, W.; Morrissey, M. M. Design, Synthesis, and Activity of a Novel Series of factor Xa Inhibitors: Optimization of Arylamidine groups. *J. Med. Chem.* **2002**, *45*, 2484–2493.
- (24) Jorgensen, W. L.; Maxwell, D. S.; Tirado-Rives, J. Development and Testing of OPLS All-Atom Force Field on Conformational Energetics and Properties of Organic Liquids. *J. Am. Chem. Soc.* **1996**, *118*, 11225–11235.
- (25) Kaminski, G. A.; Friesner, R. A.; Tirado-Rives, J.; Jorgensen, W. J. Evaluation and Reparametrization of the OPLS-AA Force Field for Proteins via Comparison with Accurate Quantum Chemical Calculations on Peptides. *J. Phys. Chem. B* **2001**, *105*, 6474–6487.
- (26) *Glide, version 5.0*, Schrödinger, LLC: New York, 2008.
- (27) *MacroModel, version 9.0*, Schrödinger, LLC: New York, 2005.
- (28) *KNIME, version 1.2*, Schrödinger, LLC: New York, 2008.
- (29) *WaterMap, version 1.0*, Schrödinger, LLC: New York, 2008.
- (30) Wong, C. F.; McCammon, J. A. Dynamics and Design of Enzymes and Inhibitors. *J. Am. Chem. Soc.* **1986**, *108*, 3830–3832.
- (31) *MCPRO+, version 1.36*, Schrödinger, LLC: New York, 2008.
- (32) Essex, J.; Jorgensen, W. L. An Empirical Boundary Potential for Water Droplet Simulations. *J. Comput. Chem.* **1995**, *16*, 9510–972.
- (33) Jorgensen, W. L.; Ravimohan, C. Monte Carlo Simulation of Differences in Free Energies of Hydration. *J. Chem. Phys.* **1985**, *83*, 3050–3056.
- (34) Boresch, S.; Karplus, M. The Role of Bonded Terms in Free Energy Simulations: I. Theoretical Analysis. *J. Phys. Chem. A* **1999**, *103*, 103–118.
- (35) Pearlman, D. A.; Kollman, P. A. The Overlooked Bond-Stretching Contribution in Free Energy Perturbation Calculations. *J. Chem. Phys.* **1991**, *94*, 4532–4545.
- (36) Price, D. J.; Jorgensen, W. L. Improved Convergence of Binding Affinities with Free Energy Perturbation: Application to Nonpeptide Ligands with pp60<sup>c-src</sup> SH2 Domain. *J. Comput.-Aided Mol. Des.* **2001**, *15*, 681–695.
- (37) Allen, M. P.; Tildesley, D. J. *Computer Simulations of Liquids*; Clarendon Press: Oxford, U.K., 1987.
- (38) Jorgensen, W. L.; Chandrasekhar, J.; Madura, J. D.; Impey, W.; Klein, M. L. Comparison of Simple Potential Functions for Simulating Liquid Water. *J. Chem. Phys.* **1983**, *79*, 926–935.
- (39) Gilson, M. K.; Davis, M. E.; Luty, B. A.; Mccammon, J. A. Computation of Electrostatics Forces on Solvated Molecules Using the Poisson-Boltzmann Equation. *J. Phys. Chem.* **1993**, *97*, 3591–3600.
- (40) Bashford, D.; Case, D. A. Generalized Born Models of Macromolecular Solvation Effects. *Annu. Rev. Phys. Chem.* **2000**, *51*, 129–152.
- (41) Jorgensen, W. L.; Ulmschneider, J. P.; Tirado-Rives, J. Free Energies of Hydration from a Generalized Born Model and an All-Atom Force Field. *J. Phys. Chem. B* **2004**, *108*, 16264–16270.
- (42) Roe, D. R.; Okur, A.; Wickstrom, L.; Hornak, V.; Simmerling, C. Secondary Structure Bias in Generalized Born Solvent Models: Comparison of Conformational Ensembles and Free Energy of Solvent Polarization from Explicit and Implicit Solvation. *J. Phys. Chem. B* **2007**, *111*, 1846–1857.
- (43) Gallicchio, E.; Kubo, M. M.; Levy, R. M. Enthalpy-Entropy and Cavity Decomposition of Alkane Hydration Free Energies: Numerical Results and Implications for Theories of Hydrophobic Solvation. *J. Phys. Chem. B* **2000**, *104*, 6271–6285.
- (44) Pitera, J. W.; van Gunsteren, W. F. The Importance of Solute-Solvent van der Waals Interactions with Interior Atoms of Biopolymers. *J. Am. Chem. Soc.* **2001**, *123*, 3163–3164.
- (45) Brown, S. P.; Muchmore, S. W.; Hajduk, P. J. Healthy Skepticism: Assessing Realistic Model Performance. *Drug Discovery Today* **2009**, *14*, 420–427.
- (46) Pearlman, D. A.; Charifson, P. S. Are Free Energy Calculations Useful in Practice? A Comparison with Rapid Scoring Functions for the p38 MAP Kinase Protein System. *J. Med. Chem.* **2001**, *44*, 3417–3423.
- (47) Murray, C. W.; Verdonk, M. L. The Consequences of Translational and Rotational Entropy Lost by Small Molecules on Binding to Proteins. *J. Comput.-Aided Mol. Des.* **2002**, *16*, 741–753.
- (48) Chang, C. A.; Chen, W.; Gilson, M. K. Ligand Configurational Entropy and Protein Binding. *Proc. Natl. Acad. Sci. U.S.A.* **2007**, *104*, 1534–1539.

CI900497D